Organic Geochemistry 70 (2014) 10–19

Contents lists available at ScienceDirect

Organic Geochemistry

journal homepage: www.elsevier.com/locate/orggeochem

Tetraether lipids from the southern Yellow Sea of China: Implications for the variability of East Asia Winter Monsoon in the Holocene

Huangmin Ge [a], Chuanlun L. Zhang [a,*], Jun Li [b,*], Gerard J.M. Versteegh [c], Bangqi Hu [b], Jingtao Zhao [b], Liang Dong [a]

[a] State Key Laboratory of Marine Geology, Tongji University, Shanghai 200092, China
[b] Key Laboratory of Marine Hydrocarbon Resources and Environmental Geology, Qingdao Institute of Marine Geology, Ministry of Land and Resources, Qingdao 266071, China
[c] Heisenberg Group on Marine Kerogen, Center for Marine Environmental Sciences (MARUM), Bremen University, D 28359 Bremen, Germany

ARTICLE INFO

Article history:
Received 7 November 2013
Received in revised form 9 February 2014
Accepted 11 February 2014
Available online 22 February 2014

ABSTRACT

To better understand the origin and distribution of organic matter (OM) in the Yellow Sea (YS) and to delineate potential interactions between the atmosphere and the marine system during the Holocene, we reconstructed terrestrial input and temperature variation for the last 8.8 ka BP, using glycerol dialkyl glycerol tetraethers (GDGTs) obtained from a 4.4 m sediment core (YSC-1) from the southern YS. The archaea-derived isoprenoid GDGTs (iGDGTs) were dominated by GDGT-0 and crenarchaeol. The iGDGTs and bacteria-derived branched GDGTs (bGDGTs) correlated well and varied in opposition to the BIT (branched vs. isoprenoid tetraether) index. This may be due to varying river runoff and influence of the YS Coastal Current (YSCC) and YS Warm Current (YSWC), related to the East Asia Winter Monsoon (EAWM), which made the BIT proxy less suitable for tracing soil OM input to the YS. TEX_{86} (tetraether index of tetraethers consisting of 86 carbons)-derived sea surface temperature values (SST) varied from 9 to 16 °C, close to the SST in the YS cold season. The MBT/CBT (methylation of branched tetraethers and cyclization of branched tetraethers)-derived continental temperature ranged from 10 to 19 °C, indicating an annual mean air temperature for the middle and low drainage basin of the YS. These two temperature records were decoupled but both correlated with the variation in the EAWM, suggesting an intimate link between EAWM and temperature variation in East Asia.

1. Introduction

Marginal seas are complex and dynamic transitional zones between land and ocean. They are the major marine realms for organic matter (OM) burial (Hedges and Keil, 1995; Wagner and Dupont, 1999) and are of significant interest for global carbon cycle studies (e.g. Wollast, 1998; Onstad et al., 2000). Understanding of marginal sea dynamics through time may be enhanced by using well calibrated temperature proxies to reconstruct past environments and delineate natural climate regulatory mechanisms (Schouten et al., 2008a,b; Blaga et al., 2010; Bendle et al., 2010; Fallet et al., 2012).

Since marginal seas record both marine and terrestrial changes, they are especially well suited for reconstructing past climate. An important variable in global transport of heat and moisture is monsoon systems, which also have a strong impact on vegetation cover, river dynamics and sediment transport (e.g. Chen, 2009; Sun et al., 2011). They also affect the marine environment indirectly through riverine input of sediments and modification of nutrients, sediment and salinity, or directly through wind driven changes in circulation (e.g. Jian et al., 2000; Liu et al., 2006; Wu et al., 2012). The climate of East Asia is dominated by such a monsoon system, with SE winds leading to warm and wet summers and NW winds resulting in cold and dry winters (e.g. Xiang et al., 2008; Liu et al., 2009; Xing et al., 2012; Hu et al., 2012).

Glycerol dialkyl glycerol tetraethers (GDGTs) are major membrane lipids of microorganisms. Isoprenoid GDGTs (iGDGTs) are produced by marine and terrestrial archaea, while branched GDGTs (bGDGTs) are produced predominantly by soil bacteria (c.f. Schouten et al., 2013). GDGTs respond to environmental change, allowing development of proxies for studying past climate and environment. TEX_{86} (tetraether index of tetraethers consisting of 86 carbons) is commonly used to reconstruct mean annual sea surface temperature (SST). It is based on the distribution of iGDGTs synthesized by pelagic Thaumarchaeota (e.g. Schouten et al., 2002, 2013; Kim et al., 2008, 2010; Brochier-Armanet et al., 2008; Spang et al., 2010; Pearson and Ingalls, 2013). It has both global and local calibrations for SST (e.g. Schouten et al., 2002, 2013; Kim et al., 2008, 2010; Trommer et al., 2009; Jia et al.,

* Corresponding authors. Tel.: +86 21 65987697 (C.L. Zhang).
E-mail addresses: archaea.zhang@gmail.com (C.L. Zhang), junli741001@gmail.com (J. Li).

http://dx.doi.org/10.1016/j.orggeochem.2014.02.011
0146-6380/

2012; Kabel et al., 2012). Although TEX_{86}-derived temperature values are commonly interpreted as annual SST (e.g. Huguet et al., 2006b; Blaga et al., 2011), they have also been considered to reflect summer SST in the open ocean (Leider et al., 2010; Castañeda et al., 2010; Shintani et al., 2011), winter SST in the shallow waters near ocean margins (Leider et al., 2010; Wei et al., 2011; Ge et al., 2013), or sub-surface temperature (Huguet et al., 2007; Lopes dos Santos et al., 2010; Richey et al., 2010; Jia et al., 2012; Li et al., 2013).

The BIT (branched vs. isoprenoidal tetraether) index is a proxy for the relative contributions of soil vs. aquatic sedimentary OM (Hopmans et al., 2004; Walsh et al., 2008; Schouten et al., 2013). It was established to characterize the terrestrial OM input to the marine system because bGDGTs were considered to be solely soil derived (e.g. Hopmans et al., 2004; Weijers et al., 2006). Recent studies have shown, however, that bGDGTs are also produced in situ in marine environments (Peterse et al., 2009a), lakes (e.g. Sinninghe Damsté et al., 2009; Tierney et al., 2010), estuaries (Zhu et al., 2011; Zhang et al., 2012) and hot springs (Hedlund et al., 2013; Zhang et al., 2013).

The MBT (methylation of branched tetraethers) and CBT (cyclization of branched tetraethers) proxies are used to estimate soil pH and annual mean air temperature (MAT), respectively (Weijers et al., 2007a). They have also been applied to study past continental climate and environment using marginal marine sediment cores, taking advantage of the fact that the bGDGTs were transported from land to ocean by rivers (Hopmans et al., 2004; Weijers et al., 2007a) or by ice rafting events (Schouten et al., 2007b, 2008a,b). As records from marginal settings represent signals integrated over a whole drainage basin (Weijers et al., 2007b; Blaga et al., 2010), the extent to which the continental climate is reflected in the MBT/CBT proxy is unclear (Peterse et al., 2009a,b). Furthermore, the combined use of TEX_{86} and MBT/CBT for climate reconstruction has yet to be demonstrated.

To better understand the East Asian Monsoon system and its impact on the marginal Yellow Sea (YS), we analyzed a sediment core from this region with respect to its GDGT composition and derived an environmental reconstruction for most of the Holocene using TEX_{86}-derived SST, MBT/CBT-derived MAT, and BIT. The specific objectives of the study were to (i) reveal the abundance and distribution of GDGTs and to explore environmental signals revealed by GDGT-derived proxies, e.g. TEX_{86}, MBT/CBT and BIT, (ii) better understand the origin and distribution of OM in the YS and (iii) delineate potential interactions between climate, sea level and the marine system in this transitional area, with special attention to the variation in the EAWM. The importance of the YS Warm Current (YSWC) is emphasized because it partially reflects the strength of the EAWM.

2. Regional setting

The YS is connected to the Japan/East Sea via the Korea and Tsushima Straits and opens indirectly to the western Pacific Ocean via the East China Sea (Fig. 1). It has a maximum water depth of 140 m (avg. 44 m; Feng et al., 2004; Liu et al., 2009) and an annual SST of 15 °C. It is influenced significantly by terrestrial input, particularly through the Yellow River and Yangtze River that flow through several climate zones and bring in OM with a mixed signal (e.g. Yang et al., 2002).

The YS is also significantly affected by complex seasonal currents (Fig. 1). The present circulation is characterized by a counterclockwise gyre with the northwestward warm and salty YSWC and low salinity southward YS Coastal Current (YSCC) moving along the western Chinese coast (e.g. Park et al., 2000; Yang et al., 2003). The YSWC is a branch of the Tsushima Current and compensates for the export of water, driven out of the YS as the YSCC by the Northern West winds during the EAWM. A stronger winter monsoon thus results in a more prominent tongue and northward penetration into the YS of warm and salty YSWC water. As such, a warming period reconstructed from a location sensitive to the YSWC influence may thus indicate a stronger EAWM. The YS water column is vertically homogeneous in winter, due to vertical convection and strong wind stirring caused by the EAWM, and highly stratified in summer as a result of the combined effects of surface heat, riverine input and a cold bottom YSCW (cf. Wei et al., 2010).

The basin-wide cyclonic gyre created by the YSWC and the YSCC has resulted in the formation of the largest mud deposition area in the central basin of the YS, which has attracted considerable attention concerning its sediment provenance and depositional processes (Zhao et al., 1990, 2001; Park and Khim, 1992; Park et al., 2000; Yang et al., 2003). Mixed sources such as riverine input, marine OM and coastal erosion from the old Yellow River Delta, have been suggested for the central mud deposits of the YS according to geochemical evidence, including grain size, carbonate composition and total organic carbon, clay mineral assemblage, and elemental concentrations and ratios (e.g. Zhao et al., 1990; Hu et al., 1998; Saito, 1998; Yang et al., 2003 and references therein).

In general, the Yellow River contributes most of the sediment to the YS (Qin and Li, 1983; Milliman et al., 1987; Qin et al., 1989; Lee and Chough, 1989; Alexander et al., 1991; Park and Khim, 1992; Yang and Liu, 2007). However, it has been suggested recently that the fine sediment in the central mud region is not derived from the Yellow River, but most likely is a mixture of sediments from the Yangtze River and small rivers in the Korean Peninsula (Li, J., et al., unpublished results).

A postglacial stepwise sea level rise dominated the sedimentary processes in the YS during the Late Quaternary (Kim and Kucera, 2000; Liu et al., 2004; Kong et al., 2006; Xiang et al., 2008; Xing et al., 2012). Three periods were distinguished: low sea level from 12.5 to 11.5 ka BP, rising sea level from 11.5 to 7 ka BP and high sea level from 7 ka BP to the present (e.g. Lee and Chough, 1989; Milliman et al., 1989; Lee and Yoon, 1997; Kim et al., 1999). According to the benthic foraminiferal assemblage (low salinity species such as *Ammonia aomoriensis and Ammonia beccarii*, and less brackish and deeper waters species such as *Ammonia ketienziensis* and *Astrononion italicum*), the Holocene YS had a shallow coastal environment affected by fresh water and an associated input of terrestrial organic carbon before ca. 7.9 (Kim and Kennett, 1998) or 6.9 (Xiang et al., 2008) ka BP and a modern marine shelf environment with higher salinity, higher marine productivity and lower terrestrial OM input after ca. 7.5 (Kim and Kennett, 1998) or 6–5 (Xiang et al., 2008) ka BP. An important role in this development was played by the YSWC when sea level was high enough for it to enter the YS around 6.5–6 ka BP (Liu et al., 1999, 2007; Wang et al., 2009) or 4.3–3.5 ka BP (Kong et al., 2006).

3. Material and methods

3.1. Material

Core YSC-1 (length 4.4 m, water depth 76.2 m; Fig. 1) was collected at 123°40′E and 35°39′N, stored in a −20 °C freezer upon collection and then allowed to thaw to room temperature before sampling; 80 samples were collected at different depth intervals for lipids analysis. The grain size and dating data used are from Li, J., et al. (unpublished results).

3.2. Lipid extraction

The protocol is a modification of that from Huguet et al. (2010). In short, an aliquot (ca. 10 g) of the freeze dried and homogenized

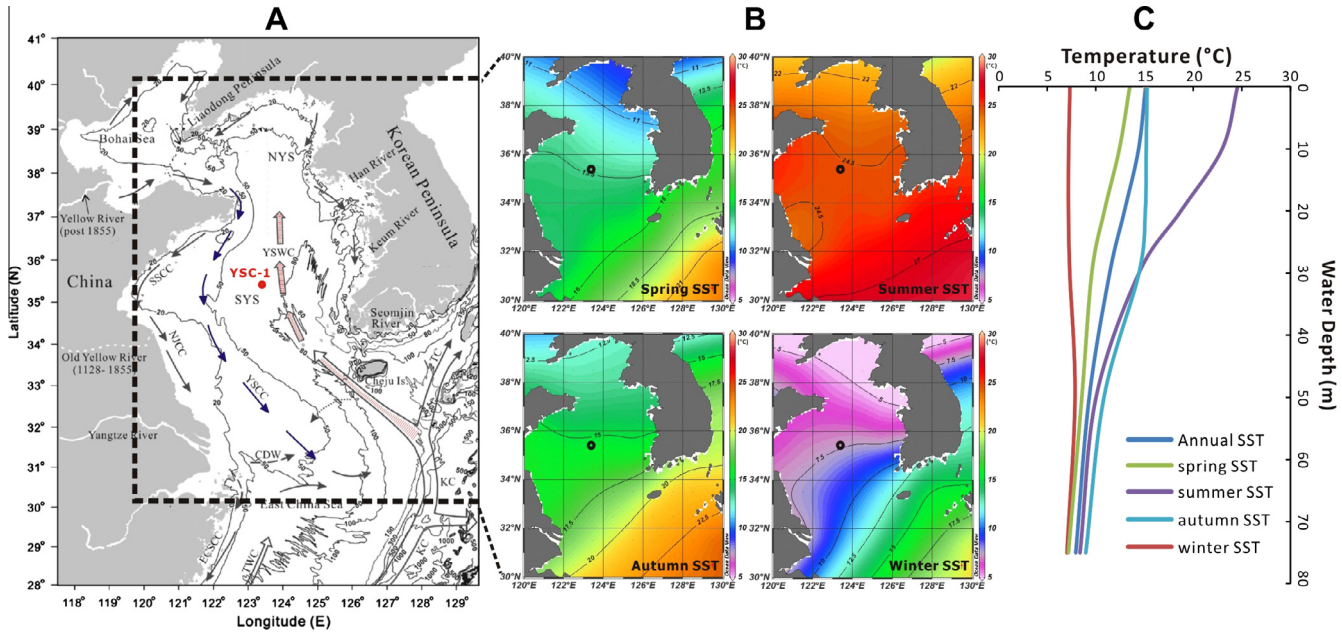

Fig. 1. Map of east coastal seas of China with bathymetry and water circulation patterns in winter [A, modified from Liu et al. (2009)], seasonal sea surface temperature (SST) in dotted rectangular area (B) including the Yellow Sea (YS) and adjacent continents and the northern part of the East China Sea, and the instrumental annual and seasonal temperatures at different water depths (0–75 m) at the site location in this work (C). The red circle in the left panel and black circles in the middle panels indicate location of YSC-1. Water depth is shown in m. Other labels: NYS, North Yellow Sea; SYS, South Yellow Sea; YSWC, Yellow Sea Warm Current; YSCC, Yellow Sea Coastal Current; KC, Kuroshio Current; TC, Tsushima Current; TWC, Taiwan Warm Current; SKCC, South Korean Coastal Current; NJCC, North Jiangsu Coastal Current; SSCC, South Shandong Coastal Current; CDW, Yangtze River Diluted Water; ECSCC, East China Sea Coastal Current (for interpretation of the references to color in this figure legend, the reader is referred to the web version of this article).

sediment sample was spiked with a known amount internal standard (C_{46} GDGT; 974 ng; Huguet et al., 2006a) and extracted ultrasonically for 15 min with dichloromethane (DCM)/MeOH (3:1, v/v;5x) and MeOH (1x). With each extraction, the sample was centrifuged at 3000 rpm for 3 min to remove particles. All supernatants were combined and the solvent was removed under a N_2 stream.

The total lipid extract (TLE) was dissolved in 3 ml hexane:isopropanol (99:1, v/v) and 1 ml of the mixture was filtered through a 0.45 μm PFTE filter. The solvent was removed from the filtered TLE with a N_2 stream and the residue dissolved in 300 μl hexane:isopropanol (99:1, v/v), of which 5 μl were used for lipid analysis.

3.3. GDGT analysis and calculation of proxies

Analysis of GDGTs was performed using high performance liquid chromatography–mass spectrometry (HPLC–MS) with an Agilent 1200 high HPLC instrument with an automatic injector coupled to QQQ 6460 mass spectrometer and with mass hunter LC–MS manager software, following a method modified from Hopmans et al. (2004) and Schouten et al. (2007a). Detailed parameters and procedures followed those from Ge et al. (2013). A Prevail Cyano column (2.1 × 150 mm, 3 μm; Alltech, Deerfield, Illinois, USA) was used with an Agilent 6460 triple quadrupole mass spectrometer under atmospheric pressure chemical ionization (APCI) conditions. All procedures were performed using gradient elution with hexane and isopropanol.

GDGTs were detected using the single ion monitoring (SIM) mode included six iGDGTs (m/z 1302, 1300, 1298, 1296, and 1292 and its isomer), seven bGDGTs (m/z 1050 1036, 1034, 1032, 1022, 1020, 1018) and the internal standard C_{46} GDGT (m/z 744) (Fig. A1), with a dwell time of 237 ms per ion. The bGDGTs with m/z 1048 and 1046 were below detection limit. Quantification was achieved by integrating the area of each $[M+H]^+$ peak.

The formulae used for calculating the GDGT-referred proxies were:

(i) TEX_{86} (Schouten et al., 2002) and TEX_{86}-derived SST (TEX_{86}^H is the logarithmic function of TEX_{86}, Kim et al., 2010):

$$TEX_{86} = \frac{GDGT-2 + GDGT-3 + Cren'}{GDGT-1 + GDGT-2 + GDGT-3 + Cren'}$$

$$SST = 68.4 \times TEX_{86}^H + 38.6$$

(ii) BIT (Hopmans et al., 2004):

$$BIT = \frac{I + II + III}{I + II + III + Cren}$$

(iii) MBT, CBT and their derived MAT (Weijers et al., 2007a):

$$MBT = \frac{I + Ib + Ic}{I + Ib + Ic + II + IIb + IIc + III + IIIb + IIIc}$$

$$CBT = -\log\frac{Ib + IIb}{I + II}$$

$$T_{MBT/CBT} = (MBT - 0.122 - 0.187 \times CBT)/0.02$$

3.4. Instrumental temperature data

The annual and seasonal composite sea surface temperature (SST) values were obtained from the World Ocean Atlas 2009 (WOA09) provided by Schlitzer, R., Ocean Data View, http://odv.awi.de, 2010 (Fig. 1).

4. Results

4.1. iGDGTs and bGDGTs

The iGDGTs were dominated by GDGT-0 and crenarchaeol, both of which ranged from 28 to 280 ng/g dry sediment. GDGTs-1, -2

and -3 each stayed below 15 ng/g dry sediment. The concentration of total bGDGTs ranged from 16 to 140 ng/g dry sediment, with a relatively higher concentration in bGDGTs-I, -Ib, -Ic, -II, -IIb and -III, and a lower concentration of bGDGT-IIc. GDGT-IIIb and -IIIc were not detected. The total iGDGTs and bGDGTs showed a similar trend in the past 8.8 ka BP (Fig. 2 left and Fig. 3), which could be divided into three periods (Fig. 3). Period A, from 8.8–6.4 ka BP, was characterized by relatively high GDGT concentration and wide variation therein, such as large peaks at 8.2, 7.8, 6.8 and 6.6 ka BP. Period B, from 6.4–4.0 ka BP, represented a prolonged period with generally low and stable GDGT concentration (e.g. iGDGTs averaged 106 ± 16 ng/g dry sediment). Period C, from 4.0–0.9 ka BP, began with an increase in GDGT concentration, which stayed at a higher average level than period B (they did not return to values below 140 ng/g dry sediment). Concentration also varied more dramatically again, with the highest value occurring around 1.2 ka BP. Through the whole record, crenarchaeol correlated significantly with the other iGDGTs ($R^2 > 0.8$), particularly with GDGT-0 (R^2 0.98, $p < 0.001$). The total amount of iGDGTs and bGDGTs also correlated significantly (R^2 0.91, $p < 0.001$; Fig. 2, right).

4.2. Temperature based on TEX_{86} and MBT/CBT

The temperature of the YS is around 15 °C, which suggests that TEX_{86}^{H} was potentially suitable as an SST proxy (Kim et al., 2010). SST based on TEX_{86}^{L} showed highly variable values ranging from -4.6 to 9.4 °C, possibly because TEX_{86}^{L} was more developed for polar oceans.

TEX_{86} values ranged from 0.37 to 0.46, corresponding to TEX_{86}^{H}-derived SST from 9 to 16 °C, with a mean value of 14 ± 0.8 °C ($n = 40$) in the relatively warm period (e.g. 6.5–5.3 ka BP) and a mean value of 11 ± 0.9 °C ($n = 40$) in the relatively cold period (e.g. 2.9–2.3 ka BP). Despite the fluctuation, the TEX_{86}^{H}-derived SST increased with time (except for a sudden peak around 8 ka BP) till reaching a top value at 6.4 ka BP in period A, and remained high and decreased slightly during period B. During period C, the SST decreased rapidly at first, followed by a slow increase (Fig. 4).

The MBT/CBT-derived temperature ranged from 10 to 19 °C, with a mean of 16 ± 0.8 °C ($n = 42$) in the relatively warm period (e.g. 3.6–2.9 ka BP) and a mean of 14 ± 0.9 °C ($n = 38$) in the relatively cold period (e.g. 6.9–5.9 ka BP). It showed in general an opposite trend from TEX_{86}^{H}-derived SST through the whole core (Fig. 4).

4.3. BIT index and grain size records

The BIT index (Hopmans et al., 2004) ranged from 0.14 to 0.31 (Fig. 3c). Mean grain size varied between 7.5 and 5.5 ϕ (Fig. 3d). Grain size and BIT were negatively correlated (R^2 0.37, $p < 0.001$; Supplementary Fig. 1).

5. Discussion

5.1. Possible provenance of iGDGTs and bGDGTs

The distribution of iGDGTs was characteristic of marine archaeal GDGT profiles (e.g. Menzel et al., 2006; Herfort et al., 2006b; Huguet et al., 2006b; Leider et al., 2010; Jia et al., 2012; Schouten et al., 2013). The significant correlation among different iGDGTs (Fig. 2) indicates a common source, which is most likely aquatic Thaumarchaeota. This was supported by the dominance of crenarchaeol throughout the record (52 ± 2%, $n = 80$), a ratio of GDGT-0/crenarchaeol < 1 (cf. Blaga et al., 2009) and a small (<1%) relative abundance of the crenarchaeol isomer (cf. Pitcher et al., 2011; Sinninghe Damsté et al., 2012).

Considering the proximity of land and large rivers to the YS, the bGDGTs may be considered to be land-derived. The CBT-derived pH (7.7 ± 0.2, $n = 80$) based on the new calibration from Peterse et al. (2012) matched well with the measured mean pH value of 7.80 for the middle reaches of the Yellow River (cf. Ran, 2013), while the MBT/CBT-derived temperature record (see next section) was also consistent with the MAT data for the middle and low reaches of the Yellow River drainage basin. The successful application of the two soil calibrations supports a soil origin for the bGDGTs.

The observed covariance between iGDGT and bGDGT concentrations may be explained through covariance between riverine nutrient input and marine productivity, as reported for GDGTs in other regions (e.g. Sinninghe Damsté et al., 2009; Leider et al., 2010; Fietz et al., 2011b; Grauela et al., 2013; Schouten et al., 2013; Wu et al., 2013). The YS became gradually flooded during the Holocene marine transgression, which reached its maximum sea level around 7 ka BP (Kim et al., 1999 and references therein). Period A in our record represents a coastal/estuarine environment characterized by a large amount of fresh water, low salinity and associated input of terrestrial organic matter (e.g. Kim and Kennett, 1998; Xiang et al., 2008; Hu et al., 2012). Therefore, the fluctuating

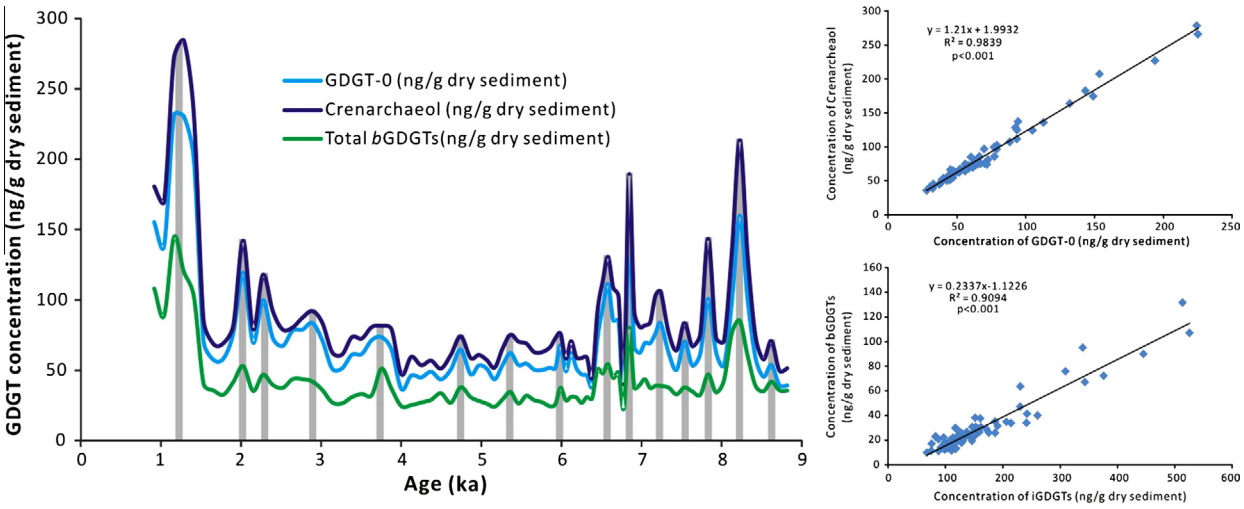

Fig. 2. *Left:* Abundance of GDGT-0, crenarchaeol and total bGDGTs in the downcore sediments (the past 8.8 ka) from the southern Yellow Sea. *Right:* Relationship between the abundances of GDGT-0 and crenarchaeol (top), and between total iGDGTs and bGDGTs (bottom).

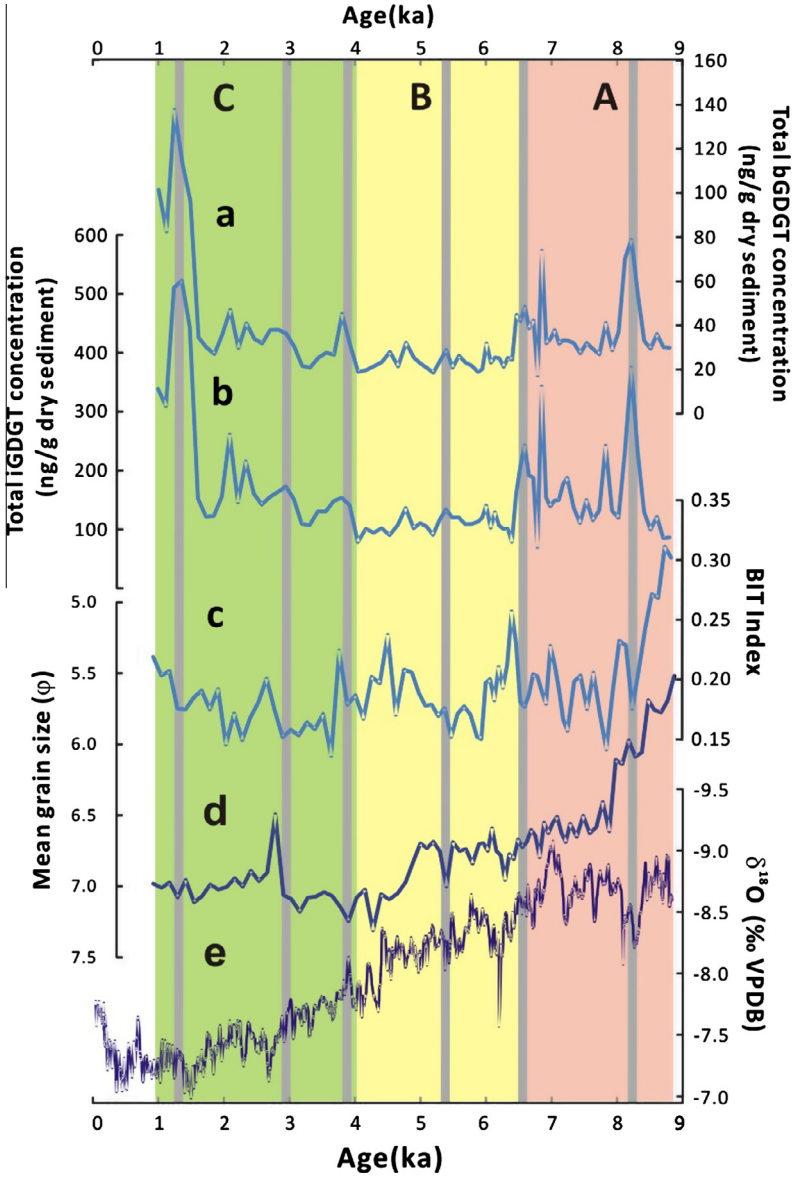

Fig. 3. Total bGDGT concentration (a), total iGDGT concentration (b), BIT index (c), and mean grain size (d) from YSC-1 for the past 8.8 ka. The $\delta^{18}O$ record from a stalagmite in the Hulu Cave (e) is from Wang et al. (2005). Three periods (A, B, C) are separated according to the variation in GDGT concentration and covered in light pink, yellow, and green, respectively. The shaded gray bars indicate several points with high GDGT concentration and low BIT values (for interpretation of the references to color in this figure legend, the reader is referred to the web version of this article).

but high bGDGT concentration in period A is interpreted as reflecting the proximity of rivers and periodic maxima in fluvial runoff. The low concentration of GDGTs in period B agrees with a stable modern marine shelf sedimentary environment with higher salinity due to the intrusion of open ocean water (e.g. Kim and Kennett, 1998; Xiang et al., 2008; Hu et al., 2013) and lower terrestrial OM input because of weak summer precipitation since the middle Holocene (Yuan et al., 2004; Dykoski et al., 2005; Wang et al., 2005). The weak East Asia Summer Monsoon (EASM) is characterized by less precipitation, which therefore reduces the input of the continental signal to the marine system through river flow, leading to a low bGDGT concentration in period B. Both iGDGTs and bGDGTs increased slowly in period C till peak values occurred around 1.2 ka BP, which might be attributed to flooding events. A partially negative correlation between GDGT concentration and EAWM (Figs. 3 and 4) indicates that a more vigorous EAWM led to less deposition of GDGTs at our core site, which probably resulted from the transport of terrestrial material southward along the YS coastline by the YSCC, instead of to the depocenter, and from inflow of relatively warm but oligotrophic water to the research area by the YSWC.

Finally, degradation or sediment diagenesis could impact the concentration profiles of both bGDGTs and iGDGTs, potentially causing them to vary in a similar way in concentration downcore. One way to address this question is to examine the down core variation in total organic carbon (TOC), with a decreasing pattern showing the possibility of degradation. Unfortunately, TOC data were not obtained. On the other hand, even if the bGDGTs and iGDGTs were affected by degradation, the effect appears to be equal for both types of GDGTs and does not seem to change the above overall interpretations.

The BIT index in our work seems less credible for revealing the soil contribution as it is affected more likely by the concentration of crenarchaeol than bGDGTs, which may be complicated by intertwining influences of varying river runoff and the YSCC and YSWC related to the EAWM. On the other hand, the BIT and mean grain

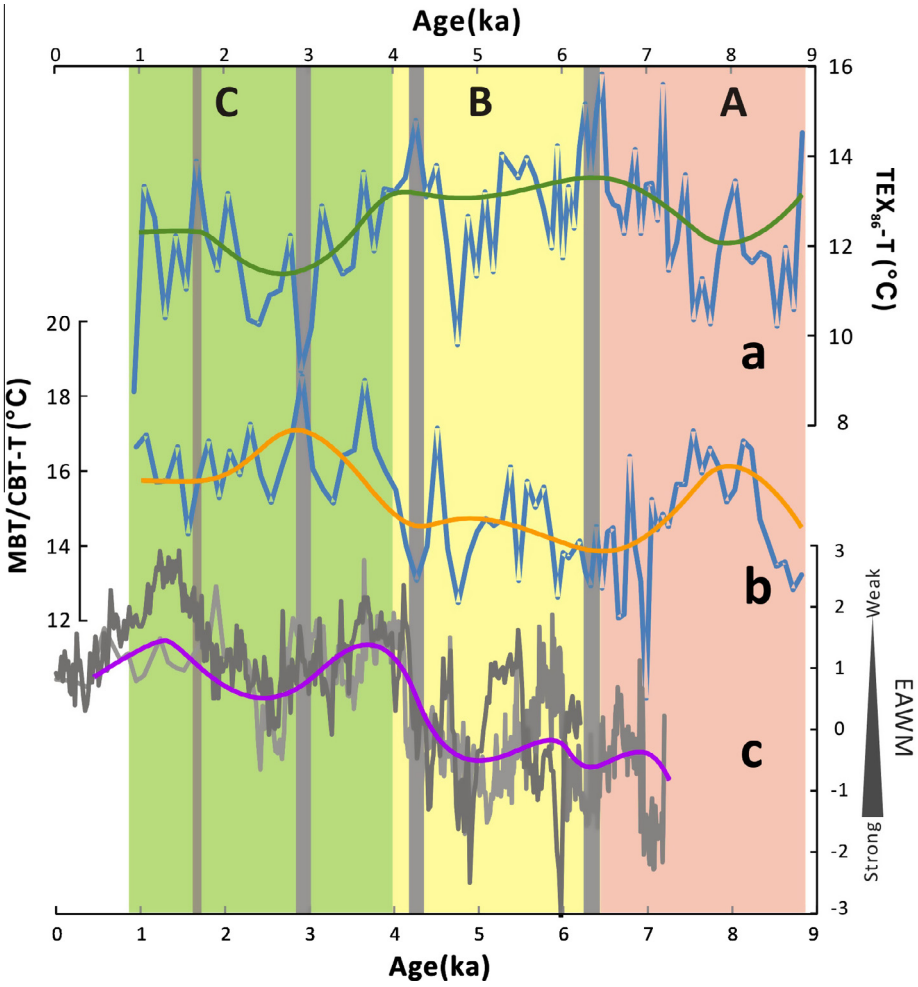

Fig. 4. Temperature records derived from TEX_{86}^{H} (a) and MBT/CBT (b) from this study, and East Asia Winter Monsoon index based on grain size analysis (c) from Hu et al. (2012). Three periods (A, B, C) are separated according to the variation in GDGT concentration and are colored in light pink, yellow, and green, respectively. The shaded gray bars highlight the correlation among the three records (for interpretation of the references to color in this figure legend, the reader is referred to the web version of this article).

size had a definite opposite trend through the whole record (Fig. 3), which indicates that the BIT is helpful for revealing the intensity history of the EAWM. Similarly, Kim et al. (2007) found that BIT was applicable for detection of flood events in coastal oceans, together with the concentration of GDGTs, which might imply a promising use of this proxy.

5.2. The EAWM and TEX_{86}- and MBT/CBT-derived temperature records

Sea surface temperature and air temperature from the same archive are valuable for understanding the interactions between ocean circulation and land climate (Rueda et al., 2009). The annual and seasonal temperatures today, derived from the World Ocean Atlas, show for the core location large differences in the upper 50 m of the water column (Fig. 1, right). During summer the temperature decreased sharply from 25 °C at the surface to about 10 °C at 50 m, while during winter the temperature in the upper 50 m was similar and around 7–8 °C. Temperature measured in spring and autumn, and the calculated annual mean temperature was about 14–15 °C at the surface and decreased only slightly downwards. All the temperature values converged at about 7–8 °C below 75 m (Fig. 1, right). On the other hand, the MAT along the Yellow River drainage basins varies from 1–8 °C in the upper reaches, 8–14 °C in the middle reaches and 12–14 °C in the lower reaches (e.g. Chen et al., 2005; Ran, 2013). Compared with the above instrumental data, the TEX_{86}^{H}-derived temperature values are closest to the winter–spring SST, while MBT/CBT-derived values are similar to MAT in the middle and low reaches of the Yellow River.

An intensified EAWM appears to correlate with both a higher TEX_{86}^{H}-derived SST and a lower MBT/CBT-derived MAT through the whole record (Fig. 4). This correlation suggests that the EAWM provides a physical link between both records, which might be explained by a close connection of the YSCC and YSWC in the YS during the EAWM (e.g. Wang et al., 2009, 2011). The southward flowing YSCC is driven by the EAWM and the excess water leaving the YS is compensated for by the northward flowing warm and salty YSWC, which, when it overlays the core site, increases TEX_{86}. Both a longer and a stronger winter monsoon may lead to a more persistent presence of the YSWC over the core site and thus a higher TEX_{86} for the sediments. The water exchange fronts caused by these two currents may increase the primary productivity and marine archaeal community (e.g. Naimiea et al., 2001; Liu et al., 2009), further strengthening the winter signal.

The bGDGT-based MBT/CBT reflects the land climate. A strong winter monsoon may result in lower MBT/CBT values in two ways. First, it increases the strength of the YSCC and therefore triggers transport of a greater contribution of northern relative to southern land-derived material to the core site. Second, it may imply an overall colder winter and thus lower mean annual temperature on land, reducing MBT/CBT in the soils of the source regions. For the latter hypothesis we may expect a time lag between TEX_{86}-derived temperature values and those from MBT/CBT related to

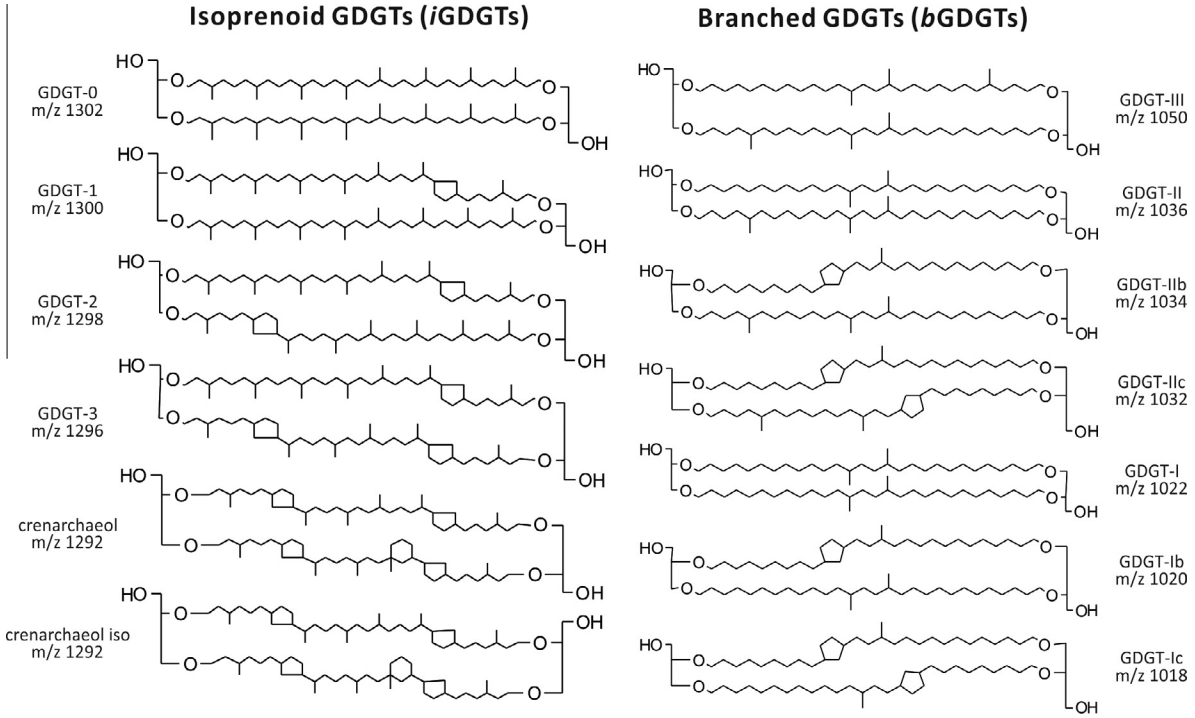

Fig. A1. Structures of iGDGTs in archaea and bGDGTs in bacteria.

leaching and transport processes involved for the bGDGTs (cf. Schouten et al., 2013). A direct response between the intensity variation of EAWM and the MBT/CBT-derived MAT, as apparent in Fig. 4, thereby supporting the former hypothesis.

The establishment of the modern circulation system in the YS is the most significant milestone in the Holocene history of this area. Its installation is disputed, especially the intrusion time of the YSWC, which might vary from 6.5 to 6.0 ka BP (Liu et al., 1999, 2007; Wang et al., 2009). Our TEX_{86}^{H}-derived temperature shows the first high values at the end of period A (8.8–6.4 ka) and we attribute the increased SST to the intrusion of the YSWC. As for its full establishment, we therefore suggest a timing prior to 6.4 ka when the TEX_{86}^{H}-derived SST reached the maximum. Grain size analysis of the same core suggests a decreased terrigenous supply from the Yangtze River to the core site from 6.4 ka (Li et al., 2013), which was also attributed to the establishment of the modern ocean circulation pattern. This is also consistent with Li et al. (2007) who reconstructed the evolution of the warm current system of the East China Sea and the YS since the last deglaciation, based on the $\delta^{18}O$ and $\delta^{13}C$ records of planktonic foraminifera and planktonic and benthic foraminiferal assemblages, as well as variation in abundance of foraminifera indicative of the Kuroshio Current and the Tsushima Warm Current.

Comparison of the GDGT concentration, mean grain size and BIT records from YSC-1 with the $\delta^{18}O$ stalagmite record from Dongge Cave, which shows variation in precipitation on the East China mainland and indicates the weakness of the East Asia Summer Monsoon (Wang et al., 2005) for the last 8.8 ka (Fig. 3), shows a close correlation of the first peak in GDGT concentration around 8.3–8.1 ka BP, coinciding with the 8.2 ka BP global cold event (Wang et al., 2005 and references therein). This event occurs during the period of relatively coarse sediment and thus a relatively strong and direct terrestrial influence. The high TEX_{86}^{H}-derived SST from 7 to 4 ka in our record suggests a strong YSWC with an intensified hydrodynamic environment, high SST in the study area and low winter temperature on land, caused by an active EAWM. However, Wang et al. (2011) show colder SST and a weaker warm current during the mid-Holocene than during the late Holocene based on an alkenone record from the nearby core ZY-2, i.e. an interpretation opposite from ours. The site of core ZY-2 is east to that of our core YSC-1. The region covering both cores is characterized by a strong oceanic front between the more eastern cold and southward flowing YSCC and the more western, warm and northward flowing YSWC (e.g. Park et al., 2000; Yang et al., 2003; Liu et al., 2009). With increasing strength of the monsoon system, the thermal gradient over this front increases. Therefore, one scenario explaining the opposite SST trends is by assuming that the ZY-2 $U_{37}^{K'}$ record reflects primarily the YSCC temperature whereas the YSC-1 TEX_{86} record reflects the YSWC. There is still an argument about the variation in EAWM in the Holocene (e.g. Yancheva et al., 2007; Hu et al., 2012), whereby the strong and highly fluctuating EAWM during 7.2–4.2 ka BP reconstructed by Hu et al. (2012) using grain size variation agrees with the intensified YSWC reconstructed by us. This event occurred during the "Holocene Climate Optimum" although its magnitude and nature are disputed and it may have been largely limited to high northern latitudes (e.g. Gagan et al., 1998; Kaufman et al., 2004). The fluctuating SST during ca. 2.0–1.0 ka BP in the period C matches the Sui and Tang dynasties warm period (cf. Wu and Dang, 1998).

Overall, a correspondence between our records and those of others emphasizes that GDGTs and the derived proxies are valuable tools for reconstruction of climate change in the YS and perhaps the East Asian continent.

6. Conclusions

The iGDGT and bGDGT distributions in core YSC-1 from the Yellow Sea support the following conclusions:

1. Covariance in the concentrations of iGDGTs and bGDGTs suggests a common environmental process, i.e. more riverine input resulting in more bGDGT input and more nutrients in the marginal marine environment, while the higher nutrient input enhances marine productivity, resulting in higher iGDGT

concentration as well. Degradation of iGDGTs and bGDGTs may also be a factor forcing the co-variation, but we lacked the TOC data to verify this possibility.

2. The TEX_{86}-derived SST and MBT/CBT-derived temperatures were close to late winter–spring SST and MAT in the middle and low reaches of the Yellow River respectively. The opposite trends between them indicate different response mechanisms, which may be related to wind direction and intensity intimately linked to EAWM variability.
3. Some global and regional events, such as the 8.2 ka BP cold event, the formation of the YSWC and the establishment of the modern current system in the Yellow Sea, and the mid-Holocene warm periods are reflected in the GDGT concentration and GDGT-based proxies, demonstrating the value of GDGT analysis for understanding past climate.

Acknowledgements

We thank two anonymous reviewers for comments, which helped improve the manuscript. We also thank Hui Wang for technical assistance during the lab work. Sediment samples were collected by the D/V KAN407 in September 2010 (cf. Li, J., et al., unpublished results). All analyses were performed at the State Key Laboratory of Marine Geology at Tongji University. The research was supported by National Key Basic Research Program of China Grant 2013CB429701 (J.L.), National Key Basic Research Program of China Grant 2013CB955700 (C.L.Z.), National Natural Science Foundation of China Grants 91028005 (C.L.Z.) and 41206049 (B.Q.H.), and the "National Thousand Talents" program through the State Key Laboratory of Marine Geology at Tongji University (C.L.Z.).

Appendix A

See Fig. A1.

Appendix A. Supplementary material

Supplementary data associated with this article can be found, in the online version, at http://dx.doi.org/10.1016/j.orggeochem.2014.02.011.

Associate Editor—**S. Schouten**

References

Alexander, C.R., DeMaster, D.J., Nittrouer, C.A., 1991. Sediment accumulation in a modern epicontinental-shelf setting: the Yellow Sea. Marine Geology 98, 51–72.

Bendle, J., Weijers, J.H.W., Maslin, M., Sinninghe Damsté, J.S., Schouten, S., Hopmans, E.C., Boot, C., Pancost, R.D., 2010. Major changes in Last Glacial and Holocene terrestrial temperatures and sources of organic carbon recorded in the Amazon fan by the MBT/CBT continental paleothermometer. Geochemistry Geophysics Geosystems 11, http://dx.doi.org/10.1029/2010GC003308.

Blaga, C.I., Reichart, G.J., Heiri, O., Sinninghe Damsté, J.S., 2009. Tetraether membrane lipid distributions in lake particulate matter and sediments: a study of 47 European lakes along a North-South transect. Journal of Paleolimnology 41, 523–540.

Blaga, C.I., Reichart, G.J., Schouten, S., Lotter, A.F., Werne, J.P., Kosten, S., Mazzeo, N., Lacerot, G., Sinninghe Damsté, J.S., 2010. Branched glycerol dialkyl glycerol tetraethers in lake sediments: can they be used as temperature and pH proxies? Organic Geochemistry 41, 1225–1234.

Blaga, C.I., Reichart, G.J., Vissers, E.W., Lotter, A.F., Anselmetti, F.S., Sinninghe Damsté, J.S., 2011. Seasonal changes in glycerol dialkyl glycerol tetraether concentrations and fluxes in a perialpine lake: implications for the use of the TEX_{86} and BIT proxies. Geochimica et Cosmochimica Acta 75, 6416–6428.

Brochier-Armanet, C., Boussau, B., Gribaldo, S., Forterre, P., 2008. Mesophilic Crenarchaeota: proposal for a third archaeal phylum, the Thaumarchaeota. Nature Reviews in Microbiology 6, 245–252.

Castañeda, I.S., Schefuß, E., Pätzold, J., Sinninghe Damsté, J.S., Weldeab, S., Schouten, S., 2010. Millennial-scale sea surface temperature changes in the Eastern Mediterranean (Nile River Delta Region) over the last 27,000 years. Paleoceanography 25, PA1208, http://dx.doi.org/10.1029/2009PA001740.

Chen, C.T.A., 2009. Chemical and physical fronts in the Bohai, Yellow and East China seas. Journal of Marine Systems 78, 394–410.

Chen, J., Wang, F., Meybeck, M., He, D., Xia, X., Zhang, L., 2005. Spatial and temporal analysis of water chemistry records (1958–2000) in the Huanghe (Yellow River) basin. Global Biogeochemical Cycles 19. http://dx.doi.org/10.1029/2004GB002325.

Dykoski, C.A., Edwards, R.L., Cheng, H., Yuan, D.X., Cai, Y.J., Zhang, M.L., Lin, Y.S., Qing, J.M., An, Z.S., Revenaugh, J., 2005. A high-resolution, absolute-dated Holocene and deglacial Asian monsoon record from Dongge Cave, China. Earth Planetary Science Letter 233, 71–86.

Fallet, U., Castañeda, I.S., Edwards, A.H., Richter, T.O., Boer, W., Schouten, S., Brummer, G.J., 2012. Sedimentation and burial of organic and inorganic temperature proxies in the Mozambique Channel, SW Indian Ocean. Deep Sea Research I 59, 37–53.

Feng, S., Li, F., Li, S., 2004. Introduction to Marine Science. Higher Education Press, Beijing (in Chinese).

Fietz, S., Martínez-Garcia, A., Huguet, C., Rueda, G., Rosell-Melé, A., 2011. Constraints in the application of the branched and isoprenoid tetraether index as a terrestrial input proxy. Journal of Geophysical Research 116, C10032. http://dx.doi.org/10.1029/2011JC007062.

Gagan, M.K., Ayliffe, L.K., Hopley, D., Cali, J.A., Mortimer, G.E., Chappell, J., McCulloch, M.T., Chappell, J., McCulloch, M.T., Head, J.M., 1998. Temperature and surface-ocean water balance of the mid-Holocene tropical western Pacific. Science 279, 1014–1018.

Ge, H., Zhang, C.L., Dang, H., Zhu, C., Jia, G., 2013. Distribution of tetraether lipids in surface sediments of the northern South China Sea: implications for TEX_{86} proxies. Geoscience Frontiers 4, 223–229.

Grauela, A.L., Leider, A., Goudeauc, M.L.S., Müller, I.A., Bernasconia, S.M., Hinrichs, K.U., Langec, G.J.D., Versteeghb, G.J.M., 2013. What do SST proxies really tell us? A high-resolution multiproxy ($U^{K'}_{37}$, TEX_{86} and foraminifera $\delta^{18}O$) study in the Gulf of Taranto, central Mediterranean Sea. Quaternary Science Reviews 73, 115–131.

Hedges, J.I., Keil, R.G., 1995. Sedimentary organic-matter preservation – an assessment and speculative synthesis. Marine Chemistry 49, 81–115.

Hedlund, B.P., Paraiso, J.J., Williams, M.J., Huang, Q., Wei, Y., Dijkstra, P., Hungate, B.A., Dong, H., Zhang, C.L., 2013. Wide distribution of autochthonous branched glycerol dialkyl glycerol tetraethers (bGDGTs) in U.S. Great Basin hot springs. Frontiers in terrestrial. Microbiology 4, 222.

Herfort, L., Schouten, S., Boon, J.P., Sinninghe Damsté, J.S., 2006b. Application of the TEX_{86} temperature proxy to the southern North Sea. Organic Geochemistry 37, 1715–1726.

Hopmans, E.C., Weijers, J.W.H., Schefuß, E., Herfort, L., Sinninghe Damsté, J.S., Schouten, S., 2004. A novel proxy for terrestrial organic matter in sediments based on branched and isoprenoid tetraether lipids. Earth and Planetary Science Letters 24, 107–116.

Hu, D., Saito, Y., Kempe, S., 1998. Sediment and nutrient transport to the coastal zone. In: Galloway, J.N., Melillo, J.M. (Eds.), Asian Change in the Context of Global Climate Change: Impact of Natural and Anthropogenic Changes in Asia on Global Biogeochemical Cycles. IGBP Book Series 3. Cambridge University Press, pp. 245–270.

Hu, B., Yang, Z., Zhao, M., Saito, Y., Fan, D., Wang, L., 2012. Grain size records reveal variability of the East Asian Winter Monsoon since the Middle Holocene in the Central Yellow Sea mud area, China. SCIENCE CHINA Earth Sciences 55, 1656–1668.

Huguet, C., Cartes, J.E., Sinninghe Damsté, J.S., Schouten, S., 2006a. Marine crenarchaeotal membrane lipids in decapods: implications for the TEX_{86} paleothermometer. Geochemistry Geophysics Geosystems. http://dx.doi.org/10.1029/2006GC001305.

Huguet, C., Kim, J.-H., Sinninghe Damsté, J.S., Schouten, S., 2006b. Application of the TEX86 temperature proxy in the reconstruction of glacial–interglacial sea surface temperature in the Arabian Sea. Paleoceanography 21, PA3003. http://dx.doi.org/10.1029/2005PA001215.

Huguet, C., Smittenberg, R.H., Boer, W., Sinninghe Damsté, J.S., Schouten, S., 2007. Twentieth century proxy records of temperature and soil organic matter input in the Drammensfjord, southern Norway. Organic Geochemistry 38, 1838–1849.

Huguet, C., Martens-Habbena, W., Urakawa, H., Stahl, D.A., Ingalls, A.E., 2010. Comparison of extraction methods for quantitative analysis of core and intact polar glycerol dialkyl glycerol tetraethers (GDGTs) in environmental samples. Limnology and Oceanography Methods 8, 127–145.

Jia, G., Zhang, J., Chen, J., Peng, P., Zhang, C.L., 2012. Archaeal tetraether lipids record subsurface water temperature in the South China Sea. Organic Geochemistry 50, 68–77.

Jian, Z., Wang, P., Saito, Y., Wang, J., Pflaumann, U., Oba, T., Cheng, X., 2000. Holocene variability of the Kuroshio Current in the Okinawa Trough, northwestern Pacific Ocean. Earth and Planetary Science Letters 184, 305–319.

Kabel, K., Moros, M., Porsche, C., Neumann, T., Adolphi, F., Andersen, T.J., Siegel, H., Gerth, M., Leipe, T., Jansen, E., Sinninghe Damsté, J.S., 2012. Impact of climate change on the Baltic Sea ecosystem over the past 1000 years. Nature Climate Change 2, 871–874, http://dx.doi.org/10.1038/nclimate1595.

Kaufman, D.S. et al., 2004. Holocene thermal maximum in the western Arctic (0–180°W). Quaternary Science Review 23, 529–560.

Kim, J.M., Kennett, J.P., 1998. Paleoenvironmental changes associated with the Holocene marine transgression, Yellow Sea (Hwanghae). Marine Micropaleontology 34, 71–89.

Kim, J.M., Kucera, M., 2000. Benthic foraminifer record of environmental changes in the Yellow Sea (Hwanghae) during the last 15,000 years. Quaternary Science Review 19, 1067–1085.
Kim, D.S., Park, B.K., Shin, I.C., 1999. Paleoenvironmental changes of the Yellow Sea during the Late Quaternary. Geo-Marine Letters 18, 189–194.
Kim, J.-H., Ludwig, W., Schouten, S., Kerhervé, P., Herfort, L., Bonnin, J., Sinninghe Damsté, J.S., 2007. Impact of flood events on the transport of terrestrial organic matter to the ocean: a study of the Têt River (SW France) using the BIT index. Organic Geochemistry 38, 1593–1606.
Kim, J.-H., Schouten, S., Hopmans, E.C., Donner, B., Sinninghe Damsté, J.S., 2008. Global core-top calibration of the TEX_{86} paleothermometer in the ocean. Geochimica et Cosmochimica Acta 72, 1154–1173.
Kim, J.-H., van der Meer, J., Schouten, S., Helmke, P., Willmott, V., Sangiorgi, F., Koç, N., Hopmans, E.C., Sinninghe Damsté, J.S., 2010. New indices and calibrations derived from the distribution of crenarchaeal isoprenoid tetraether lipids: implications for past sea surface temperature reconstructions. Geochimica et Cosmochimica Acta 74, 4639–4654.
Kong, G.S., Park, S.C., Han, H., Chang, J., Mackensen, A., 2006. Late Quaternary paleoenvironmental changes in the southeastern Yellow Sea, Korea. Quaternary International 144, 38–52.
Lee, H.J., Chough, S.K., 1989. Sediment distribution, dispersal and budget in the Yellow Sea. Marine Geology 87, 195–205.
Lee, H.J., Yoon, S.H., 1997. Development of stratigraphy and sediment distribution in the northeastern Yellow Sea during Holocene sea level rise. Journal of Sedimentary Research 67, 341–349.
Leider, A., Hinrichs, K.-U., Mollenhauer, G., Versteegh, G.J.M., 2010. Core-top calibration of the lipid-based $U^{K'}_{37}$ and TEX_{86} temperature proxies on the southern Italian shelf (SW Adriatic Sea, Gulf of Taranto). Earth and Planetary Science Letters 300, 112–114.
Li, T., Jiang, B., Sun, R., Zhang, D., Liu, Z., Li, Q., 2007. Evolution pattern of warm current system of the East China Sea and the Yellow Sea since the last deglaciation. Quaternary Sciences 27, 945–954.
Li, X., Bianchi, T.S., Allison, M.A., Chapman, P., Yang, G., 2013. Historical reconstruction of organic carbon decay and preservation in sediments on the East China Sea shelf. Journal Of Geophysical Research: Biogeosciences 118, 1–15. http://dx.doi.org/10.1002/jgrg.20079.
Liu, J., Li, S., Wang, S., Yang, Z., Ge, Z., Chang, J., 1999. Sea level changes of the Yellow Sea and formation of the Yellow sea warm current since the last deglaciation. Marine Geology & Quaternary Geology 19, 13–24.
Liu, J., Milliman, J.D., Gao, S., Cheng, P., 2004. Holocene development of the Yellow River's subaqueous delta, North Yellow Sea. Marine Geology 209, 45–67.
Liu, J., Li, A., Xu, K., Velozzia, D.M., Yang, Z., Milliman, J.D., DeMaster, D.J., 2006. Sedimentary features of the Yangtze River-derived along-shelf clinoform deposit in the East China Sea. Continental Shelf Research 26, 2141–2156.
Liu, J., Xu, K., Li, A., Milliman, J.D., Velozzi, D.M., Xiao, S., Yang, Z., 2007. Flux and fate of Yangtze River sediment delivered to the East China Sea. Geomorphology 85, 208–224.
Liu, J., Saito, Y., Kong, X., Wang, H., Zhao, L., 2009. Geochemical characteristics of sediment as indicators of post-glacial environmental changes off the Shandong Peninsula in the Yellow Sea. Continental Shelf Research 29, 846–855.
Lopes dos Santos, R., Prange, M., Castañeda, I.S., Schefuß, E., Mulitza, S., Schulz, M., Niedermeyer, E.M., Sinninghe Damsté, J.S., Schouten, S., 2010. Glacial-interglacial variability in Atlantic meridional overturning circulation and thermocline adjustments in the tropical North Atlantic. Earth and Planetary Science Letters 300, 407–414.
Menzel, D., Hopmans, E.C., Schouten, S., Sinninghe Damsté, J.S., 2006. Membrane tetraether lipids of planktonic Crenarchaeota in Pliocene sapropels of the eastern Mediterranean Sea. Palaeogeography Palaeoclimatology Palaeoecology 239, 1–15.
Milliman, J.D., Qin, Y.S., Ren, M., Saito, Y., 1987. Man's influence on the erosion and transport of sediment by Asian rivers: the Yellow River (Huanghe) example. Journal of Geology 95, 751–762.
Milliman, J.D., Qin, Y.S., Park, Y., 1989. Sediment and sedimentary processes in the Yellow and East China seas. In: Taira, A., Masuda, F. (Eds.), Sedimentary Facies in the Active Plate Margin. Terra Scientific Publishing Company, Tokyo, pp. 233–249.
Naimiea, C.E., Blainb, C.A., Lynch, D.R., 2001. Seasonal mean circulation in the Yellow Sea a model-generated climatology. Continental Shelf Research 21, 667–695.
Onstad, G.D., Canfield, D.E., Quay, P.D., Hedges, J.I., 2000. Sources of particulate organic matter in rivers from the continental USA: lignin phenol and stable carbon isotope compositions. Geochimica et Cosmochimica Acta 64, 3539–3546.
Park, Y.A., Khim, B.K., 1992. Origin and dispersal of recent clay mineral in the Yellow Sea. Marine Geology 104, 205–213.
Park, S.C., Lee, H.H., Han, H.S., Lee, G.H., Kim, D.C., Yoo, D.G., 2000. Evolution of late Quaternary mud deposits and recent sediment budget in the southeastern Yellow Sea. Marine Geology 170, 271–288.
Pearson, A., Ingalls, A.E., 2013. Assessing the use of archaeal lipids as marine environmental proxies. Annual Review of Earth and Planetary Science 41, 1–26.
Peterse, F., Kim, J.-H., Schouten, S., Klitgaard Kristensen, D., Koç, N., Sinninghe Damsté, J.S., 2009a. Constraints on the application of the MBT/CBT paleothermometer in high latitude environments (Svalbard, Norway). Organic Geochemistry 40, 692–699.
Peterse, F., van der Meer, M.T.J., Schouten, S., Jia, G., Ossebaar, J., Blokker, J., Sinninghe Damsté, J.S., 2009b. Assessment of soil *n*-alkane δD and branched tetraether membrane lipid distributions as tools for paleoelevation reconstruction. Biogeosciences 6, 2799–2807.
Peterse, F., van der Meer, J., Schouten, S., Weijers, J.W.H., Fierer, N., Jackson, R.B., Kim, J.-K., Sinninghe Damsté, J.S., 2012. Revised calibration of the MBT–CBT paleotemperature proxy based on branched tetraether membrane lipids in surface soils. Geochimica et Cosmochimica Acta 96, 215–229.
Pitcher, A., Wuchter, C., Siedenberg, K., Schouten, S., Sinninghe Damsté, J.S., 2011. Crenarchaeol tracks winter blooms of planktonic, ammonia-oxidizing Thaumarchaeota in the coastal North Sea. Limnology and Oceanography 56, 2308–2318.
Qin, Y., Li, F., 1983. Study of influence of sediment loads discharged from Huanghai Sea. In: Proceedings of the International Symposium on Sedimentation on the Continental Shelf with Special Reference to the East China Sea. Hangzhou, China, vol. 1, pp. 91–101.
Qin, Y., Zhao, Y., Chen, L., Zhao, S., 1989. Geology of the Yellow Sea. China Ocean Press, Beijing.
Ran, L., 2013. Recent Riverine Carbon of the Yellow River: Fluxes, Outgassing and Burial. PhD Thesis, National University of Singapore.
Richey, J.N., Hollander, D.J., Flower, B.P., Eglinton, T.I., 2010. Merging late Holocene molecular organic and foraminiferal-based geochemical records of sea surface temperature in the Gulf of Mexico. Paleoceanography 26, PA1209. http://dx.doi.org/10.1029/2010PA002000.
Rueda, G., Rosell-Melé, A., Escala, M., Gyllencreutz, R., Backman, J., 2009. Comparison of instrumental and GDGT-based estimates of sea surface and air temperatures from the Skagerrak. Organic Geochemistry 40, 287–291.
Saito, Y., 1998. Sedimentary environment and budget in the East China Sea. Bulletin of Coastal Oceanography 36, 43–58.
Schouten, S., Hopmans, E.C., Schefuß, E., Sinninghe Damsté, J.S., 2002. Distributional variations in marine crenarchaeotal membrane lipids: a new tool for reconstructing ancient sea water temperatures? Earth and Planetary Science Letters 204, 265–274.
Schouten, S., Huguet, C., Hopmans, E.C., Sinninghe Damsté, J.S., 2007a. Improved analytical methodology of the TEX_{86} paleothermometry by high performance liquid chromatography/atmospheric pressure chemical ionization-mass spectrometry. Analytical Chemistry 79, 2940–2944.
Schouten, S., Van Der Meer, M.T.J., Hopmans, E.C., Rijpstra, W.I.C., Reysenbach, A.L., Ward, D.M., Sinninghe Damsté, J.S., 2007b. Archaeal and bacterial glycerol dialkyl glycerol tetraether lipids in hot springs of Yellowstone National Park (USA). Applied and Environmental Microbiology 73, 6181–6691.
Schouten, S., Hopmans, E.C., Baas, M., Boumann, H., Standfest, S., Könneke, M., Stahl, D.A., Sinninghe Damsté, J.S., 2008a. Intact membrane lipids of "Candidatus Nitrosopumilus maritimus", a cultivated representative of the cosmopolitan mesophilic Group I Crenarchaeota. Applied and Environmental Microbiology 74, 2433–2440.
Schouten, S., Baas, M., Hopmans, E.C., Sinninghe Damsté, J.S., 2008b. An unusual isoprenoid tetraether lipid in marine and lacustrine sediments. Organic Geochemistry 39, 1033–1038.
Schouten, S., Hopmans, E.C., Sinninghe Damsté, J.S., 2013. The organic geochemistry of glycerol dialkyl glycerol tetraether lipids: a review. Organic Geochemistry 54, 19–61.
Shintani, T., Yamamoto, M., Chen, M., 2011. Paleoenvironmental changes in the northern South China Sea over the past 28,000 years: a study of TEX_{86}-derived sea surface temperatures and terrestrial biomarkers. Journal of Asian Earth Sciences 40, 1221–1229.
Sinninghe Damsté, J.S., Ossebaar, J., Abbas, B., Schouten, S., Verschuren, D., 2009. Fluxes and distribution of tetraether lipids in an equatorial African lake: constraints on the application of the TEX_{86} palaeothermometer and branched tetraether lipids in lacustrine settings. Geochimica et Cosmochimica Acta 73, 4232–4249.
Sinninghe Damsté, J.S., Ossebaar, J., Schouten, S., Verschuren, D., 2012. Distribution of tetraether lipids in the 25-kyr sedimentary record of Lake Challa: extracting reliable TEX_{86} and MBT/CBT palaeotemperatures from an equatorial African lake. Quaternary Science Reviews 50, 43–54.
Spang, A., Hatzenpichler, R., Brochier-Armanet, C., Rattei, T., Tischler, P., Spieck, E., Streit, W., Stahl, D.A., Wagner, M., Schleper, C., 2010. Distinct gene set in two different lineages of ammonia-oxidizing archaea supports the phylum Thaumarchaeota. Trends in Microbiology 554, 331–340.
Sun, D., Tan, W., Pei, Y., Zhou, L., Wang, H., Yang, H., Xu, Y., 2011. Late Quaternary environmental change of Yellow River Basin: an organic geochemical record in Bohai Sea (North China). Organic Geochemistry 42, 575–585.
Tierney, J.E., Russell, J.M., Eggemont, H., Hopmans, E.C., Verschuren, D., Sinninghe Damsté, J.S., 2010. Environmental controls on branched tetraether lipid distributions in tropical East African lake sediments: a new lacustrine paleothermometer? Geochimica et Cosmochimica Acta 74, 4902–4918.
Trommer, G., Sicca, M., van der Meer, M.T.J., Schouten, S., Sinninghe Damsté, J.S., Schulz, H., Hemleben, C., Kucera, M., 2009. Distribution of crenarchaeotal tetraether membrane lipids in surface sediments from the Red Sea. Organic Geochemistry 40, 724–731.
Wagner, T., Dupont, L.M., 1999. Terrestrial organic matter in marine sediments: analytical approaches and eolian-marine records in the central Equatorial Atlantic. In: Fischer, G., Wefer, G. (Eds.), Use of Proxies in Paleoceanography: Examples from the South Atlantic. Springer-Verlag, Berlin, Heidelberg, pp. 547–574.
Walsh, E.M., Ingalls, A.E., Keil, R.G., 2008. Sources and transport of terrestrial organic matter in Vancouver Island fjords and the Vancouver–Washington Margin: a multiproxy approach using $\delta^{13}C_{org}$, lignin phenols, and the ether lipid BIT index. Limnology and Oceanography 53, 1054–1063.

Wang, Y., Cheng, H., Edwards, R.L., He, Y., Kong, X., An, Z., Wu, J., Kelly, M.J., Dykoski, C.A., Li, X., 2005. The Holocene Asian monsoon: links to solar changes and North Atlantic climate. Science 308, 854–857.

Wang, L., Yang, Z., Zhao, X., Xing, L., Zhao, M., Saito, Y., Fan, D., 2009. Sedimentary characteristics of core YE-2 from the central mud area in the South Yellow Sea during last 8400 years and its interspace coarse layers. Marine Geology & Quaternary Geology 29, 1–11 (in Chinese with English abstract).

Wang, L., Yang, Z., Zhang, R., Fan, D., Zhao, M., 2011. Sea surface temperature records of core ZY2 from the central mud area in the South Yellow Sea during last 6200 years and related effect of the Yellow Sea Warm Current. Chinese Science Bulletin 56. http://dx.doi.org/10.1007/s11434-011-4442-y (in Chinese with English abstract).

Wei, H., Shi, J., Lu, Y.Y., Peng, Y., 2010. Inter annual and long-term hydrographic changes in the Yellow Sea during 1977–1998. Deep-Sea Research II 57, 1025–1034.

Wei, Y., Wang, J., Liu, J., Dong, L., Li, L., Wang, H., Wang, P., Zhao, M., Zhang, C.L., 2011. Spatial variations in Archaeal lipids of surface water and core-top sediments in the South China Sea: implications for paleoclimate studies. Applied and Environmental Microbiology 77, 7479–7489.

Weijers, J.W.H., Schouten, S., Spaargaren, O.C., Sinninghe Damsté, J.S., 2006. Occurrence and distribution of tetraether membrane in soils: implications for the use of the BIT index and the TEX_{86} SST proxy. Organic Geochemistry 37, 1680–1693.

Weijers, J.W.H., Schouten, S., van Den Donker, J.C., Hopmans, E.C., Sinninghe Damsté, J.S., 2007a. Environmental controls on bacterial tetraether membrane lipid distribution in soils. Geochimica et Cosmochimica Acta 71, 703–713.

Weijers, J.W.H., Schefuss, E., Schouten, S., Sinninghe Damsté, J.S., 2007b. Coupled thermal and hydrological evolution of tropical Africa over the last deglaciation. Science 315, 1701–1704.

Wollast, R., 1998. Evolution and comparison of the global carbon cycle in the coastal zone and in the open ocean. The Sea 10.

Wu, H., Dang, A., 1998. Fluctuation and characteristics of climate change in temperature of Sui-Tang times in China. Quaternary Sciences 1, 31–38.

Wu, W., Tan, W., Zhou, L., Yang, H., Xu, Y., 2012. Sea surface temperature variability in southern Okinawa Trough during last 2700 years. Geophysical Research Letters 39. http://dx.doi.org/10.1029/2012GL052749.

Wu, W., Zhao, L., Pei, Y., Ding, W., Yang, H., Xu, Y., 2013. Variability of tetraether lipids in Yellow River-dominated continental margin during the past eight decades: Implications for organic matter sources and river channel shifts. Organic Geochemistry 60, 33–39.

Xiang, R., Yang, Z., Saito, Y., Fan, D., Chen, M., Guo, Z., Chen, Z., 2008. Paleoenvironmental changes during the last 8400 years in the southern Yellow Sea: benthic foraminiferal and stable isotopic evidence. Marine Micropaleontology 67, 104–119.

Xing, L., Zhao, M., Zhang, H., Zhao, X., Zhao, X., Yang, Z., Liu, C., 2012. Biomarker evidence for paleoenvironmental changes in the southern Yellow Sea over the last 8200 years. Chinese Journal of Oceanology and Limnology 30, 1–11.

Yancheva, G., Nowaczyk, N.R., Mingram, J., Dulski, P., Schettler, G., Negendank, J.F.W., Liu, J., Sigman, D.M., Peterson, L.C., Haug, G.H., 2007. Influence of the intertropical convergence zone on the East Asian monsoon. Nature 445, 74–77.

Yang, Z., Liu, J., 2007. A unique Yellow River-derived distal subaqueous delta in the Yellow Sea. Marine Geology 240, 169–176.

Yang, S., Jung, H.S., Choi, M.S., Li, C., 2002. The rare earth element compositions of the Changjiang (Yangtze) and Huanghe (Yellow) river sediments. Earth and Planetary Science Letters 201, 407–419.

Yang, S., Jung, H.S., Lim, D.I., Li, C., 2003. A review on the provenance discrimination of sediments in the Yellow Sea. Earth Science Reviews 63, 93–120.

Yuan, D., Cheng, H., Edwards, R., Dykoski, C., Kelly, M., Zhang, M., Qing, J., Lin, Y., Wang, Y., Wu, J., Dorale, J., An, Z., Cai, Y., 2004. Timing, duration, and transitions of the Last Interglacial Asian Monsoon. Science 304, 575–578.

Zhang, C.L., Wang, J., Wei, Y., Zhu, C., Huang, L., Dong, H., 2012. Production of branched tetraether lipids in the Lower Pearl River and Estuary: effects of extraction methods and impact on bGDGT proxies. Frontiers in Microbiology 2, 274.

Zhang, C.L., Wang, J., Dodsworth, J.A., Williams, A.J., Zhu, C., Hinrichs, K.U., Zheng, F., Hedlund, B.P., 2013. In situ production of branched glycerol dialkyl glycerol tetraethers in a great basin hot spring (USA). Frontier in Microbiology 4. http://dx.doi.org/10.3389/fmicb.2013.00181.

Zhao, Y., Qin, Z., Li, F., Chen, Y., 1990. On the source and genesis of the mud in the central area of the south Yellow Sea. Chinese Journal of Oceanology and Limnology 8, 66–73.

Zhao, Y., Park, Y.A., Qin, J., Gao, S., Li, F., Cheng, P., Jiang, R., 2001. Material source for the Eastern Yellow Sea Mud: evidence of mineralogy and geochemistry from China-Korea joint investigations. Yellow Sea 7, 22–26.

Zhu, C., Weijers, J.W.H., Wagner, T., Pan, J.M., Chen, J.F., Pancost, R.D., 2011. Sources and distributions of tetraether lipids in surface sediments across a large river dominated continental margin. Organic Geochemistry 42, 376–386.